

# Effect of three-body elastic scattering on charm quark momentum degradation in the quark-gluon plasma

W. Liu<sup>1</sup> and C. M. Ko<sup>1</sup>

<sup>1</sup>*Cyclotron Institute and Physics Department, Texas A&M University, College Station, Texas 77843-3366*

Charm quark momentum degradation due to three-body elastic scattering in the quark-gluon plasma is studied. At temperatures reachable in heavy ion collisions at the Relativistic Heavy Ion Collider (RHIC), contribution to the charm quark drag coefficient from three-body elastic scattering is found to be comparable to those from two-body elastic and radiative scatterings. The observed large suppression of charm production at high transverse momenta can be explained if both charm quark two- and three-body scatterings are included.

PACS numbers: 12.38.Mh;24.85.+p;25.75.-q

One of the most interesting observations in central heavy ion collisions at RHIC is the suppressed production of hadrons with large transverse momentum [1, 2]. This phenomenon has been attributed to the radiative energy loss of partonic jets produced from initial hard scattering of incoming nucleons as they pass through the dense partonic matter formed in the collisions [3, 4, 5]. The same mechanism fails, however, to explain a similarly large suppression of high transverse momentum charmed mesons observed in these collisions as a result of the dead cone effect associated with massive quarks [6, 7]. Furthermore, experimental data have indicated that charm quarks develop a substantial elliptic flow in non-central heavy ion collisions at RHIC [8], consistent with that predicted by the quark coalescence model in which charm quarks are assumed to be thermalized in the quark-gluon plasma (QGP) [9]. In both the Fokker-Planck approach [10] and the transport model [11, 12], to reproduce the observed strong suppression of charm production at high transverse momentum as well as large charm elliptic flow requires a charm quark two-body elastic scattering cross section that is much larger than that given by the perturbative QCD. It has been suggested that such a large cross section might be due to the formation of colorless charmed resonances in the QGP when the charm quark scatters with a light quark [13]. On the other hand, it was recently realized [14] that two-body elastic scattering causes a similar energy loss for the charm quark as the two-body radiative scattering [15], and a large fraction of the observed suppression of charmed meson production at high transverse momentum can be accounted for when both contributions are included.

Since the density of the partonic matter formed in heavy ion collisions at RHIC is large, ranging from about  $1 \text{ fm}^{-3}$  near hadronization to more than  $10 \text{ fm}^{-3}$  during the initial stage, one thus wonders if charm quark three-body elastic scattering is also important in quark-gluon plasma. Indeed, previous studies have shown that gluon [16] and quark [17] three-body elastic scatterings are more efficient than two-body elastic scattering for the thermalization of initially produced partons. In this paper, the effect of three-body elastic scattering on charm quark energy loss in the quark-gluon plasma is studied.

We have included all allowed diagrams for charm quark ( $c$ ) scattering by quarks ( $q$ ) and antiquarks ( $\bar{q}$ ) with different flavors but only those that are expected to be important for other three-body scattering processes that involve a large number of diagrams.

For the processes  $cqq \rightarrow cqq$ ,  $c\bar{q}\bar{q} \rightarrow c\bar{q}\bar{q}$ ,  $cq\bar{q} \rightarrow cq\bar{q}$  with different quark and antiquark flavors, the charm quark can exchange either one or two gluons with the light quarks and antiquarks as shown by the two topologically different  $t$ -channel diagrams (a) and (b) in Fig. 1. While exchanging the two gluons in all possible ways but keeping only one to be exchanged by the charm quark (thick line) generates four diagrams from diagram (a), only two diagrams are generated from diagram (b), corresponding to either the left or the right gluon is first exchanged.

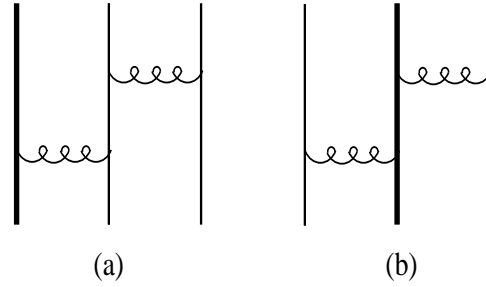


FIG. 1: Topologically different diagrams for charm quark (thick line) three-body elastic scatterings  $cqq \rightarrow cqq$  and  $c\bar{q}\bar{q} \rightarrow c\bar{q}\bar{q}$  as well as  $cq\bar{q} \rightarrow cq\bar{q}$  with different quark and antiquark flavors.

To ensure true three-body scattering, the intermediate quark in both diagrams (a) and (b) of Fig. 1 must be off-shell, and this can be achieved by replacing its mass  $m$  with  $m + i\Gamma/2$ , where  $\Gamma$  is its collisional width in the QGP, and keeping only the real part of the quark propagator in evaluating these diagrams. Similar method has previously been used to treat three-body scattering in hadronic matter [18]. The quark width in QGP is given by  $\Gamma/\hbar = \sum_i \langle \overline{|\mathcal{M}_i|^2} \rangle$ , where the sum is over all scattering processes with  $|\mathcal{M}_i|^2$  being their squared amplitudes after averaging over the spins and colors of initial partons

and summing over those of final partons. The symbol  $\langle \dots \rangle$  denotes average over the thermal distributions of scattered quarks or gluons in the quark-gluon plasma and integration over the momenta of all final-state partons, i.e.,

$$\begin{aligned} & \overline{\langle |\mathcal{M}_{i_1 \dots i_m \rightarrow j_1 \dots j_n}|^2 \rangle} \\ &= \frac{1}{2E_{i_1}} \prod_{k=2, \dots, m} \int \frac{g_{i_k} d^3 \mathbf{p}_{i_k}}{(2\pi)^3 2E_{i_k}} \prod_{l=1, \dots, n} \int \frac{d^3 \mathbf{p}_{j_l}}{(2\pi)^3 2E_{j_l}} \\ & \times \prod_{k=2, \dots, m} f(\mathbf{p}_{i_k}) \prod_{l=2, \dots, n} [1 \pm f(\mathbf{p}_{j_l})] \overline{|\mathcal{M}_{i_1 \dots i_m \rightarrow j_1 \dots j_n}|^2} \\ & \times (2\pi)^4 \delta^{(4)} \left( \sum_{k=1, \dots, m} p_{i_k} - \sum_{l=1, \dots, n} p_{j_l} \right) \end{aligned} \quad (1)$$

where  $g$  and  $E$  are the degeneracy and energy of a particle,  $f(\mathbf{p})$  is the thermal distribution, and the  $+$  and  $-$  signs in  $1 \pm f$  are for gluons and quarks, respectively.

We first consider the quark width due to two-body elastic and radiative scatterings as well as the inverse process of the latter. For charm quark two-body elastic scattering, there is only one  $t$ -channel gluon-exchange diagram for the process  $cq \rightarrow cq$  or  $c\bar{q} \rightarrow c\bar{q}$ , while there are in addition one  $s$ -channel charm quark pole and one  $u$ -channel charm quark exchange diagram for the process  $cq \rightarrow cg$ . For two-body radiative scattering, its diagrams can be obtained from those for charm quark two-body elastic scattering by allowing the gluon to be radiated from any one of external partons, the exchanged gluon, or the triple gluon vertex, generating altogether 5 diagrams for the process  $cq \rightarrow cqg$  or  $c\bar{q} \rightarrow c\bar{q}g$  and 16 diagrams for the process  $cq \rightarrow cgg$ . For the light quark, there are additional diagrams besides those similar to the ones for charm quark, and all these diagrams are included in our calculations. In evaluating these diagrams, we remove the collinear singularity in  $t$ -channel diagrams by using a screening mass  $m_D = gT$  [19], where  $g$  is the QCD coupling constant and  $T$  is the temperature of the QGP, for the exchanged gluon, and the infrared singularity in two-body radiative scattering by including the thermal mass  $m_g = m_D/\sqrt{2}$  [19] of radiated gluon.

Using the QCD coupling  $\alpha_s = g^2/4\pi = 0.3$ , appropriate for the energy scales considered here and also including the thermal mass for all time-like gluons as well as the thermal mass  $m_g = m_D/\sqrt{6}$  [19] for time-like light quarks, we find that both the charm and light quark collisional widths in the QGP increase almost linearly with the quark momentum and the temperature of the QGP. For a charm quark of momentum  $4 \text{ GeV}/c$ , its width in the QGP increases from about 75 MeV at  $T = 175$  MeV to about 130 MeV at  $T = 350$  MeV. Most of this width is due to two-body elastic scattering with only about 25% from two-body radiative scattering and its inverse process. For light quark, its width is about 50% larger than that of charm quark. Using above calculated quark widths in the intermediate quark propagator in the diagrams of Fig. 1, we find that three-body elastic scat-

tering with quarks and antiquarks increases the quark width by at most 10% and can thus be neglected. We note that since the charm quark width  $\Gamma_c < m_g$ , i.e., the time between charm quark collisions is longer than the time for radiating a thermal gluon, the destructive Landau-Pomeranchuk-Migdal (LPM) interference effect [20], which is neglected in present study, is small for charm quark two-body radiative scattering.

In the Fokker-Plank approach, the momentum degradation of a charm quark in the QGP depends on its drag coefficient. As shown in Refs.[13, 21], the drag coefficient  $\gamma(|\mathbf{p}|, T)$  of a charm quark of momentum  $\mathbf{p}$  is given by averages similar to that in Eq.(1), i.e.,  $\gamma(|\mathbf{p}|, T) = \langle |\mathcal{M}|^2 \rangle - \langle |\mathcal{M}|^2 \mathbf{p} \cdot \mathbf{p}' \rangle / |\mathbf{p}|^2$ , where  $\mathbf{p}'$  is the momentum of the charm quark after scattering.

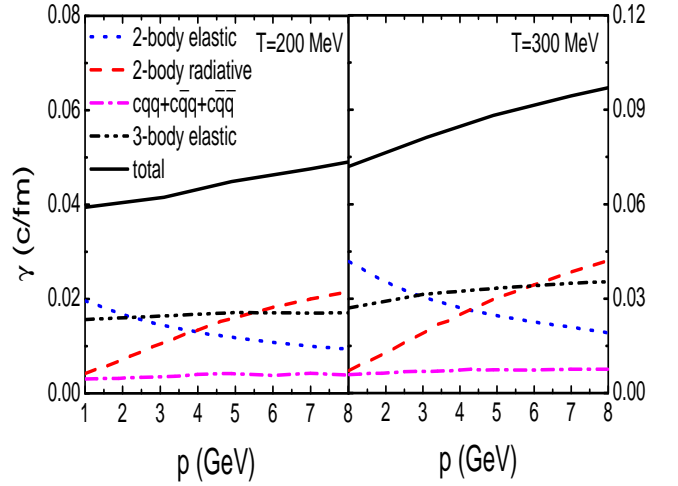


FIG. 2: Charm quark drag coefficients due to two-body elastic (dotted line) and radiative (dashed line) scatterings, and three-body elastic scattering by quarks and gluons (dash-dotted line) as well as their sum (solid line) as functions of its momentum in a QGP of temperature  $T = 200$  MeV (left panel) or  $T = 300$  MeV (right panel). The dash-dotted line is the charm quark drag coefficient due to three-body elastic scattering by light quarks and antiquarks with different flavors.

In Fig. 2, we show the charm quark drag coefficient as a function of its momentum in QGP at temperatures  $T = 200$  MeV (left panel) and  $T = 300$  MeV (right panel). It is seen that the contribution from three-body scattering by light quarks and antiquarks with different flavors (dash-dotted line) is non-negligible compared to those from two-body elastic (dotted line) and radiative scatterings (dashed line). We note that the contribution from diagram (b) of Fig. 1 with the charm quark exchanging two gluons is almost one order of magnitude large than that due to diagram (a) of Fig. 1 with the charm quark exchanging only one gluon.

If the two light quarks or antiquarks in Fig. 1 have same flavor, the number of diagrams is then doubled by the presence of additional diagrams obtained by inter-

changing the final two light quarks or antiquarks. These exchange diagrams give same contribution as that due to diagrams (a) and (b) of Fig. 1. For the process  $cq\bar{q} \rightarrow cq\bar{q}$  with same quark and antiquark flavor, besides diagrams similar to those of Fig. 1, the quark and antiquark can annihilate to a time-like virtual gluon, giving rise to additional five diagrams corresponding to different ways a gluon is exchanged between the charm quark and the light quark, antiquark, and time-like gluon. The contribution from these annihilation diagrams is found to be small, and this allows us to neglect the interference terms between these diagrams and the diagrams in Fig. 1. Neglecting also the interference terms between above direct and exchange diagrams for scattering by two identical quarks or antiquarks, the contribution from quarks and antiquarks with same flavor is then the same as that for quarks and antiquarks with different flavors.

For charm quark three-body elastic scattering involving gluons, there are 36 diagrams for the processes  $cqg \rightarrow cqg$  or  $c\bar{q}g \rightarrow c\bar{q}g$ , and 123 diagrams for the process  $cgg \rightarrow cgg$ . We have not been able to evaluate all these diagrams. Instead, we assume that these processes are also dominated by diagrams similar to diagram (b) of Fig. 1. This is partially justified as for the process  $ggg \rightarrow ggg$ , we have found that the result obtained by including thermal and screening masses in the Parke formula [22] that takes into account many diagrams with different topologies from that of diagram (b) of Fig. 1 indeed shows that their contribution to the quark drag coefficient is much smaller than that due to diagram (b) of Fig. 1. Within this approximation, the contribution from  $cgg \rightarrow cgg$  to the charm quark drag coefficient is slightly smaller while that from  $cqg \rightarrow cqg$  and  $c\bar{q}g \rightarrow c\bar{q}g$  is about a factor of three larger than that due to scattering by quarks and antiquarks, essentially due to the associated color and flavor factors in these processes. Because of the importance of  $cqg \rightarrow cqg$  and  $c\bar{q}g \rightarrow c\bar{q}g$ , the charm quark width due to three-body elastic scattering is significantly increased compared to that due to three-body scattering by quarks and antiquarks. Including this additional width to the intermediate charm quark in diagram (b) of Fig. 1 leads to a charm quark drag coefficient due to three-body elastic scattering (dash-dot-dotted line in Fig. 2) that is comparable to those due to two-body elastic or radiative scattering. The resulting total drag coefficient for charm quarks due to both elastic two- and three-body scattering is shown by the solid line in Fig. 2.

To see the effect of three-body elastic scattering on charm quark momentum degradation in QGP, we consider central Au+Au collisions at center-of-mass energy of  $\sqrt{s_{NN}} = 200$  GeV. At midrapidity, the initial transverse momentum spectrum of charm quarks is taken to be  $dN_c/d^2p_T \propto [1 + p_T/(3.25\text{GeV}/c)]^{-8}$  with  $p_T$  in  $\text{GeV}/c$  as in Ref.[12], based on experimental data from d+Au collisions at same energy [23]. These charm quarks are further assumed to be produced uniformly in the QGP with their transverse momentum pointing isotropically in the transverse plane.

For the dynamics of formed QGP, we assume that it evolves boost invariantly in the longitudinal direction but with an accelerated transverse expansion. Specifically, its volume expands in proper time  $\tau$  according to  $V(\tau) = \pi R(\tau)^2 \tau$ , where  $R(\tau) = R_0 + a/2(\tau - \tau_0)^2$  is the transverse radius with an initial value of  $R_0 = 7$  fm,  $\tau_0 = 0.6$  fm is the QGP formation time, and  $a = 0.1c^2/\text{fm}$  is the transverse acceleration [24]. With an initial temperature of  $T_i = 350$  MeV, this model gives a total transverse energy comparable to that measured in experiments. The time dependence of the temperature is then obtained from entropy conservation, dropping to the critical temperature of  $T_c = 175$  MeV at proper time  $\tau_c = 5$  fm.

For charm quarks created in the transverse position  $\mathbf{r}$  with an angle  $\phi$  relative to their transverse momentum  $\mathbf{p}_0$ , time evolution of their mean transverse momentum  $\langle p_T \rangle$  can be obtained from the Fokker-Planck equation, i.e.,  $d\langle p_T \rangle/dt = -\langle \gamma(p_T, T) p_T \rangle$ . To solve this equation, we note that the momentum dependence of the charm quark drag coefficient shown in Fig. 2 can be approximately parametrized by  $\gamma(p_T, T) = \gamma_0(T)[1 + ap_T]$ . We then have  $d\langle p_T \rangle/dt \approx -\gamma_0(\langle p_T \rangle + a\langle p_T^2 \rangle) \approx -\gamma_0(\langle p_T \rangle + a\langle p_T \rangle^2)$ . In obtaining the last step, we have used the approximation  $\langle p_T^2 \rangle \approx \langle p_T \rangle^2$ , which is valid for high transverse momentum charm quarks as considered here. The final mean transverse momentum after passing through the expanding QGP is then given by  $\langle p_T \rangle = B/(1 + aB)$ , where  $B = p_0 \exp(-\int_0^{L/c} \gamma_0(\tau') d\tau')/(1 + ap_0)$  with  $L = [R(\tau)^2 - r^2 \sin^2 \phi]^{1/2} - r \cos \phi$  denoting the mean transverse path length traversed by these charm quarks in the expanding quark-gluon plasma. In the above, we have taken the velocity of charm quark to be that of light as we are interested in charm quarks with transverse momentum much larger than their masses. The final transverse momentum spectrum of charm quarks is obtained by averaging over their initial spatial and transverse momentum distributions.

Experimentally, only non-photonic electrons from charmed meson decays have been measured. We therefore need first to convert charm quarks to charmed mesons. This is usually achieved via either the independent fragmentation model [25] or the coalescence model [9, 12]. In both cases, the resulting charmed meson transverse momentum is not too different from that of charm quarks. We thus take the two to be the same for simplicity. Electrons from decays of these charmed mesons via  $D^- \rightarrow K^0(K^{*0})e^- \bar{\nu}_e$  and  $\bar{D}^0 \rightarrow K^+(K^{*+})e^- \bar{\nu}_e$  are then obtained using the Monte Carlo method.

The experimental data are usually presented in terms of the nuclear modification factor  $R_{AA}$ , which is defined by the ratio of the electron transverse momentum spectrum from final charmed mesons to that from initially produced ones. Results from our study are shown in Fig. 3. The dotted line denotes results from charm quark two-body elastic scattering only, while the dashed line is from including also charm quark two-body radiative scattering. As in Ref.[14], the effect from two-body elastic scattering on charm quark momentum degradation is

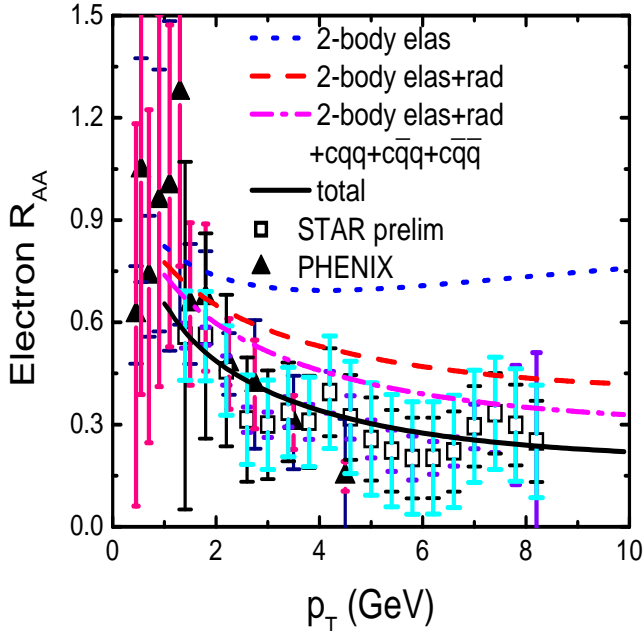


FIG. 3: Nuclear modification factor  $R_{AA}$  for electrons from charmed mesons.

as important as that from two-body radiative scattering. The experimental data from the PHENIX collaboration (filled triangles) [27] as well as the preliminary ones from the STAR collaboration (open squares) [26] show, however, a smaller charm quark nuclear modification factor than that due to charm quark two-body elastic and radiative scatterings. Including the contribution from charm quark three-body elastic scattering leads to a nuclear modification factor for charm quarks that is in excellent

agreement with the measured one as shown by the solid line in Fig. 3. If we include only charm quark three-body scattering by light quarks and antiquarks of different flavors, which is more reliably computed in present study, the resulting nuclear modification factor for charm quarks is shown by the dash-dotted line in Fig. 3, which still lies on the upper error bars of experimental data.

In the present study, we have not considered the contribution of electrons from the decay of mesons with bottom quarks. Although the number of bottom mesons produced in heavy ion collisions at RHIC is small compared to that of charmed mesons, their contribution to high transverse momentum electrons is not insignificant. Subtracting these electrons from the experimental data would lead to an even smaller measured nuclear modification factor for charm quarks than shown in Fig. 3 [28]. In this case, inclusion of charm quark three-body elastic scattering is even more essential for understanding the experimental data.

The effect of charm quark three-body scattering with gluons is evaluated in the present study using the assumption that it is dominated by  $t$ -channel gluon exchange diagrams similar to diagram (b) of Fig. 1 for three-body scattering by quarks and antiquarks with different flavors. Although we have shown that this is a valid approximation for charm quark scattering by quarks and antiquarks, its validity in scattering by gluons remains to be checked.

We wish to thank Hendrik van Hees and Ralf Rapp for useful conversations and Bin Zhang for helpful communications. This work was supported in part by the US National Science Foundation under Grant No. PHY-0457265 and the Welch Foundation under Grant No. A-1358.

---

[1] A. Adcox *et al.* [PHENIX Collaboration], Phys. Rev. Lett. **88**, 022301 (2002).  
[2] C. Adler *et al.* [STAR Collaboration], Phys. Rev. Lett. **89**, 202301 (2002); **90**, 082302 (2002).  
[3] X.N. Wang, Phys. Lett. B **579**, 299 (2004).  
[4] M. Gyulassy, P. Lévai, and I. Vitev, Phys. Rev. Lett. **85**, 5535 (2001).  
[5] U.A. Wiedemann, Nucl. Phys. B **588**, 303 (2000).  
[6] Y.L. Dokshitzer and D.E. Kharzeev, Phys. Lett. B **519**, 199 (2001).  
[7] M. Djordjevic, M. Gyulassy, and S. Wicks, Phys. Rev. Lett. **94**, 112301 (2005).  
[8] S.S. Adler *et al.* (PHENIX Collaboration), Phys. Rev. C **72**, 024901 (2005).  
[9] V. Greco, C.M. Ko, and R. Rapp, Phys. Lett. B **595**, 202 (2004).  
[10] G.D. Moore and D. Teaney, Phys. Rev. C **71**, 064904 (2005).  
[11] D. Molnar, J. Phys. G **31**, S421 (2005).  
[12] B. Zhang, L.W. Chen, and C.M. Ko, Phys. Rev. C **72**, 024906 (2005).  
[13] H. van Hees and R. Rapp, Phys. Rev. C **71**, 034907 (2005).  
[14] S. Wicks *et al.*, nucl-th/0512076.  
[15] M.G. Mustafa *et al.*, Phys. Lett. B **428**, 234 (1998).  
[16] X.M. Xu *et al.*, Nucl. Phys. A **744**, 347 (2004).  
[17] X.M. Xu, P. Ru, and H.J. Weber, Phys. Lett. B **629**, 68 (2005).  
[18] G. Batko, J. Randrup, and T. Vetter, Nucl. Phys. A **536**, 786 (1992).  
[19] J.P. Blaizot and E. Iancu, Phys. Rep. **359**, 355 (2002).  
[20] M. Djordjevic and M. Gyulassy, Nucl. Phys. A **733**, 265 (2004).  
[21] B. Svetitsky, Phys. Rev. D **37**, 2484 (1988).  
[22] M. Mangano and S.J. Parke, Phys. Rep. **200**, 301 (1991).  
[23] J. Adams *et al.* [STAR Collaboration], Phys. Rev. Lett. **94**, 062301 (2005).  
[24] L.W. Chen *et al.*, Phys. Lett. B **601**, 34 (2004).  
[25] R.V. Gavai *et al.*, Int. J. Mod. Phys. A **10**, 2999 (1995).  
[26] J. Bielcik [STAR Collaboration], nucl-ex/0511005.  
[27] S.S. Adler [PHENIX Collaboration], nucl-ex/0510047.  
[28] M. Djordjevic *et al.*, Phys. Lett. B **632**, 81 (2006).